

Jets in Micro-Quasar SS 433: Analysis involving Acceleration

Sanjay M Wagh and Sanjay B Sarwe*

Central India Research Institute, 34, Farmland, Ramdaspath, Nagpur 440010, India

Abstract

We analyze multi-wavelength observations of the jets of the micro-quasar SS 433 reported by Marshall, vis-à-vis the acceleration dependence of the Doppler Effect as reported by Wagh. Specifically, we are only interpreting the spectral shifts as arising due to the acceleration-dependent Doppler Effect and find the speed of blue-shifted jet to be $\sim 0.022c$ and that of red-shifted jet to be $\sim 0.29c$. Our results have consequences for the energetics of the prime mover and jets in SS 433.

Keywords: Doppler shift; Velocity and acceleration; Jets in SS 433

Introduction

Micro-quasar SS 433 shows [1-3] emission lines of jets from compact object. Ha Doppler shifts led Margon and Anderson [4] to the kinematic model of SS 433 as a pair of oppositely directed, processing, jets with speed $V_j \sim 0.26$. It has, since then, been used in analyzing data on SS 433, although its parameters as well as the model got updated to include nutation with a period of about half the orbital period and small variations in the jet velocity [5]. The distance to SS 433 is argued [5] to be either 5.5 ± 0.2 kpc or somewhat smaller [6] as 4.61 ± 0.35 kpc.

Margon and Anderson [4] determined jet orientation as processing with a 162.5 day period in a cone with half angle of 19.85° about an axis that is at 78.83° to the line of sight to SS 433. The jet lines are Doppler shifted with this period with the extreme red-shift being ~ 0.15 and the extreme blue-shift being ~ -0.08 as per this analysis.

Marshall et al. [7] report multi-wavelength study of jets of SS 433 using Chandra High Energy Transmission Grating Spectrometer with contemporaneous optical and VLBI observations. It is usual [4] to assume that Doppler shifts arise because of the source velocity, only. Then, assuming furthermore two perfectly oppositely directed jets at an angle θ to the line of sight, the line Doppler shifts of SS 433 are used to estimate [1,4,7,8] the relativistic γ factor and the angular factor $\mu = \cos \theta$, which are then used to determine the jet velocity and the angle to the line of sight.

To the best of our knowledge, no study is known to have focused on the role of acceleration for the jets in SS 433. It is therefore our aim here to explore it.

In what follows, we then analyze Doppler-shifted lines of SS 433 from Marshall et al. [7] and Marshall et al. [8] vis-à-vis the acceleration-dependence of the Doppler Effect [9]. We are only interpreting line shifts using the acceleration-dependence of the Doppler Effect; and are not modeling the jets in SS 433.

Acceleration and Doppler Shift

Recently, Wagh [9] showed that the Doppler shift of a source must include contribution from its acceleration, apart from that due to its velocity, and discussed [10,11] some of its direct implications.

Wagh [12] has also discussed how measurements of velocity and acceleration of the source can be effected from the Doppler shifts of its spectral lines. Cases of constant and temporally (sinusoidal) variable acceleration have, then, been analyzed in Wagh [12].

Jets from a prime mover impinge on external clouds that emit spectral lines. Then, the jet material emitted by the prime mover at a later instant should push material emitted by it at an earlier instant, against the obstruction by cloud. This leads to approximately sinusoidal temporal variability of acceleration, in the manner of a railway engine pushing a train of carriages. Then, jets should show time variable acceleration, in general.

In either case, pushing accelerates and friction decelerates. Sinusoidal variability of acceleration should then be first approximation for the above two situations.

Now, if we were to analyze the situation of jets assuming constant acceleration, we can expect to have overestimated acceleration. It will turn out that this is indeed the case in the analysis of jets in the system of SS433.

When the source S is moving (towards observer O in Figure 1 with

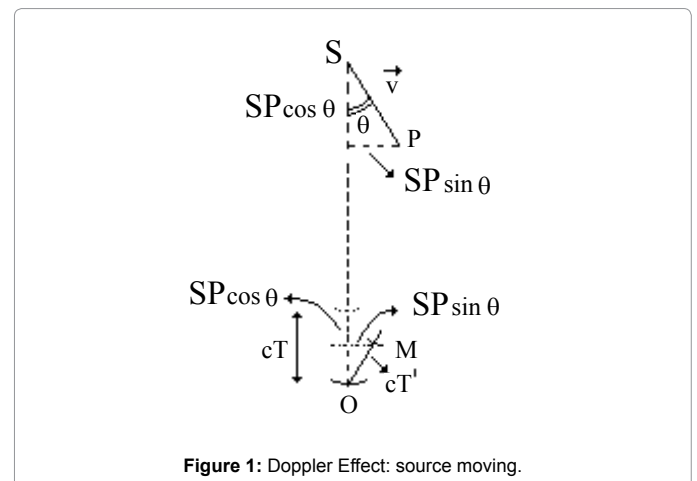


Figure 1: Doppler Effect: source moving.

*Corresponding author: Dr. Sanjay B Sarwe, S F S College, Seminary Hill, Nagpur 440006, India, Tel: +91 712 246163; E-mail: waghsm.ngp@gmail.com

Received February 27, 2014; Accepted May 03, 2014; Published June 06, 2014

Citation: Wagh SM, Sarwe SB (2014) Jets in Micro-Quasar SS 433: Analysis involving Acceleration. J Astrophys Aerospace Technol 2: 104. doi:10.4172/2329-6542.1000104

Copyright: © 2014 Wagh SM, et al. This is an open-access article distributed under the terms of the Creative Commons Attribution License, which permits unrestricted use, distribution, and reproduction in any medium, provided the original author and source are credited.

velocity v making an angle θ with the line SO and with acceleration a , we can write:

$$(MO)^2 = c^2 T'^2 = c^2 T^2 + 2cT(SP)\cos\theta + (SP)^2 \quad (1)$$

Where (SP) is the distance covered by the source in time T , c is the speed of light (in vacuum), T is the period of the wave emitted by the source, and T' is the measured period, all in the frame of observer.

We evaluate (SP) as follows. Let the temporal rate of acceleration be given by

$$\frac{da}{dt} = a_0 \sin(\omega t), \quad a_0 = \text{constant} \quad (2)$$

Then, on integration and assuming that the frequency ω is appropriately small, we obtain

$$(SP) = \frac{a_0}{\omega^3} - \left(k_1 - \frac{a_0}{\omega}\right) \frac{t^2}{2} + k_2 t + k_3 \quad (3)$$

Where k_1, k_2, k_3 are integration constants.

Substituting this in eq. (1), we then obtain after suitable manipulations:

$$v_o \approx f(\beta, \theta) v_e - \left(\frac{a_0}{c\omega^3}\right) v_e^2 \cos\theta + \left(\frac{a_0}{2c\omega}\right) \cos\theta \quad (4)$$

Where $v_o = 1/T'$ is the observed frequency, $v_e = 1/T$ is the emitted frequency, $f(\beta, \theta)$ is as defined below with $k_2 = \beta c$, and we have retained only first order terms in acceleration. We set $k_1 = 0$ and $k_3 = 0$. (We recover the case of constant acceleration when $k_1 \neq 0$ and $a_0 = 0$.)

The function

$$f(\beta, \theta) \approx 1 - \frac{\beta^2}{2} \sin^2 \theta - \beta \cos \theta \quad (5)$$

has the following characteristics. See Figure 2

For angular ranges $\sim [0, 110^\circ]$ and $\sim [240^\circ, 360^\circ]$, we have $f(\beta, \theta) < 1$; and within the angular range $\sim [110^\circ, 240^\circ]$, we have $2 \geq f(\beta, \theta) > 1$. (That $f > 1$ does not necessarily mean relativistic velocity. These ranges also overlap: for $[90^\circ, 110^\circ]$ and $[250^\circ, 270^\circ]$, $f > 1$ and $f < 1$ both.) When $f(\beta, \theta) \neq 1$, there exists a non-zero lower bound, β_{min} , for velocity β . For, $\beta_{min} = 0$, as $\beta = 0$ for all values of angle θ . (Note that for $f < 1$, $\beta_{min} = 1 - f$ and for $f > 1$, $\beta_{min} = f - 1$). Importantly, for $f(\beta, \theta) \approx 1$, velocity can be non-

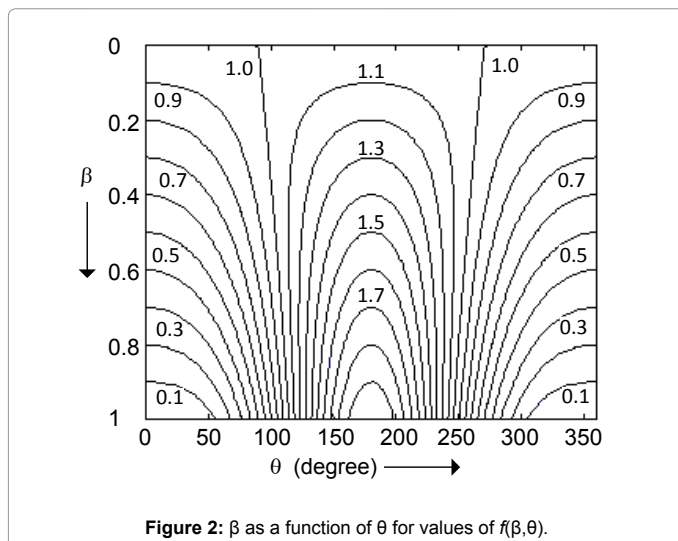


Figure 2: β as a function of θ for values of $f(\beta, \theta)$.

relativistic over quite large angular range, we may also note here.

Let source emit two spectral lines of rest frequencies $v_{e(1)}$ and $v_{e(2)}$ with corresponding observed frequencies being $v_{o(1)}$ and $v_{o(2)}$ respectively.

Now, let $\Delta v_o = v_{o(1)} - v_{o(2)}$,

$$\Delta v_e = v_{e(1)} - v_{e(2)}$$

$$\Delta(v_e^2) = v_{e(1)}^2 - v_{e(2)}^2$$

Then, from eq. (4), we have

$$\frac{\Delta v_o}{\Delta v_e} = f(\beta, \theta) + h(a_0, \omega, \theta) \left(\frac{\Delta(v_e^2)}{\Delta v_e} \right) \quad (6)$$

where we have set $h(a_0, \omega, \theta) = -\left(\frac{a_0}{\omega^3 c}\right) \cos\theta$.

Equation (6) is, evidently, linear in $\frac{\Delta v_o}{\Delta v_e}$ and $\left(\frac{\Delta(v_e^2)}{\Delta v_e}\right) \equiv v_{e(1)} + v_{e(2)}$.

From the observational data (v_e, v_o) or, equivalently, (λ_e, λ_o) where λ are the corresponding wavelengths, we can then obtain $f(\beta, \theta)$ and $h(a_0, \omega, \theta)$ by linear regression. The acceleration, $\frac{a_0}{\omega}$, of the emitter can then be estimated from the observational data.

Velocity β_{min} , corresponding to above $f(\beta, \theta)$, gives us the minimum speed at which matter emitting frequency $v_{e(1)}$ could be moving with. For the mean jet speed, β_j we may select average $\langle \beta_{min} \rangle$ of β_{min} or maximum of β_{min} . But, angle to the line of sight will be zero for any β_{min} as the velocity of the line emitting material.

Therefore, the selected value $\langle \beta_{min} \rangle$, or max (β_{min}) , is added to each β_{min} to obtain line-speeds β_L . Then, angle θ can be obtained from the f -value of each line using:

$$\cos\theta = \frac{1}{\beta_L} \left(1 - \sqrt{1 - \beta_L^2 + 2(f-1)} \right) \quad (7)$$

The jet speed is then the average of these line speeds β_L . We therefore obtain observational values of kinematical parameters of the material of the jet.

We then note that, for $a_0 = 0$, the Left Hand Side of eq. (6) directly yields $f(\beta, \theta)$, as $h(a_0, \omega, \theta)$. The value of acceleration k_1 , which is constant, is then to be obtained from eq. (4) with $k_1 \neq 0$ replacing $\frac{a_0}{\omega}$ in its last term. This value is unreasonable for the jet in SS 433 as it implies that jet material halts instantaneously. See later.

Nevertheless, we note the following. The order of the term $\frac{\Delta v_o}{\Delta v_e}$ is unity and so is that of $f(\beta, \theta)$. Then, as the order of $\left(\frac{\Delta(v_e^2)}{\Delta v_e}\right)$ is $10^8 c$, the order of $h(a_0, \omega, \theta)$ is $10^{-8} c^{-1}$. Thus, the acceleration $\frac{a_0}{\omega}$ is of order $10^{-8} \omega^2$, which yields reasonable value. (The last term of eq. (4) will then be negligible). The time-scale of change in velocity is, now, of the order of

$$\frac{\beta c}{\left(\frac{a_0}{\omega}\right)} \approx \beta c \times 10^8 / \omega^2$$

Temporally (sinusoidal) variable acceleration thence allows, in general, reasonable value(s) for the magnitude of acceleration in the jet system.

The aforementioned summarizes the role of acceleration in Doppler shift(s) of spectral lines from a source. As will be seen in the next section, the function $f(\beta, \theta)$ clearly identifies (by way of f being

greater than 1 for such lines) certain blue-shifted lines of SS 433 as being emitted by the material beyond angle of 90° to the line of sight.

The role of acceleration-dependence of Doppler Effect is therefore an important one for the analysis not only of astronomical jet situations but in general, also.

In what follows, we adopt the above strategy to analyze data on Doppler-shifted spectral lines of jets in SS 433 from Marshall et al. [7] and Marshall et al. [8].

Jets in SS433

Consider therefore Table 4 of Marshall et al. [7] reporting various blue-shifted spectral lines from the micro-quasar SS 433 with their observed and rest wavelengths. (The rest wavelengths have been computed for blends by applying weights equal to the fractional flux contribution to the blend, according to the multi-temperature plasma model). We use these data in the following analysis performed as per the details outlined in Section 2.

Firstly, of significance is the value of acceleration that we get, namely, a $\sim 10^{28}$ cm/s², when assuming constant acceleration and analyzing data in Table 4 of Marshall et al. [7] as per the corresponding

discussion in Wagh [12]. If the material of the jet were free-streaming with velocity $v_j \sim 10^9$ cm/s and encountering this deceleration, then it would be brought to rest almost instantaneously in time $\sim 10^{18}$ s! This is a certain indication that the material of the jet is also being pushed through the obstructing matter as it propagates through. That is to say, the material of the jet emitting blue-shifted lines cannot be free-streaming, and the mechanism of its acceleration is operating within the emission regions of these lines.

For these above reasons, we question the assumption of the constancy of acceleration, also. This issue was discussed in Section 2. We therefore also obtain justification for the procedure outlined in Section 2, then.

Results of our analysis (following Section 2, now) of the data on SS 433 in Table 4 of Marshall et al. [7] are given in Table 1 for jet speed $\beta_j \sim 0.022$ and in Table 2 for jet speed $\beta_j \sim 0.076$. Notice that every spectral line with $f > 1$ has $\theta \geq 90^\circ$.

Figure 3 then compares angular plots of line-velocities β for $\beta_j \sim 0.022$ and $\beta_j \sim 0.076$. Data points are fitted with cubic spline curves.

We then find the blue-shifted jet of SS 433 to be angularly limited

Identity	$\lambda_o(\text{\AA})$	$\lambda_r(\text{\AA})$	hxc	f	β	θ (deg)	a_0/w^3
Ni-XXVIII	1.532	1.526 ± 0.005	0.08903135	0.935532	0.075639	33	-0.10583205
Ni-XXVII	1.592	1.590 ± 0.002	0.08267751	0.939096	0.072075	34	-0.09912994
Fe-XXVI	1.780	1.786 ± 0.001	0.05108051	0.960209	0.050963	40	-0.06630088
Fe-XXV	1.855	1.860 ± 0.001	0.03133152	0.975514	0.035657	47	-0.04627725
Fe-XXIII	8.815	8.851 ± 0.010	0.02612262	0.988381	0.022791	60	-0.05211100
Ni-XIX	12.435	12.426 ± 0.010	0.01795082	0.989686	0.021485	62	-0.03805716
Si-XIIlr	6.648	6.652 ± 0.002	0.00838549	0.991826	0.019346	66	-0.02022888
Ar-XVII (S-XVI)	3.962	3.970 ± 0.004	0.00938674	0.992918	0.018253	68	-0.02469117
Ar-XVIII	3.733	3.740 ± 0.003	0.00871313	0.993540	0.017632	69	-0.02428936
Ni-XXVI	9.075	9.080 ± 0.004	0.00971661	0.993659	0.017513	69	-0.02741428
Ne-X	12.134	12.146 ± 0.006	0.01102429	0.994347	0.016825	71	-0.03355997
Ca-XX	3.020	3.025 ± 0.005	0.00643031	0.994555	0.016616	71	-0.02008114
S-XVI	4.729	4.735 ± 0.001	0.00438256	0.995105	0.016067	73	-0.01473865
Ca-XIX	3.187	3.191 ± 0.004	0.00445602	0.996212	0.014959	76	-0.01810022
Fe-VIII	15.014	15.021 ± 0.029	0.00639499	0.996579	0.014592	77	-0.02810862
Si-XIV	6.182	6.186 ± 0.001	0.00296826	0.996812	0.014359	78	-0.01379550
Si-XIV	5.217	5.224 ± 0.006	0.00661529	0.997036	0.014135	78	-0.03260272
Ni-XXIII	9.529	9.538 ± 0.006	0.00431469	0.997556	0.013615	80	-0.02495843
Ni-XXVI	9.745	9.737 ± 0.007	-0.00096485	0.998554	0.012618	84	0.00890177
Si-XIIlf	6.740	6.735 ± 0.004	-0.00369856	0.998642	0.012530	84	0.03618465
O-VIII	16.006	16.022 ± 0.013	0.00091487	0.999368	0.011804	87	-0.01919415
Fe-XXIII(XXII)	11.753	11.778 ± 0.008	0.00016857	1.000772	0.011944	94	0.00238848
Ni-XXVI(XXV)	9.372	9.371 ± 0.005	-0.00353610	1.000885	0.012057	95	-0.04453187
Ni-XXVI	9.970	9.973 ± 0.003	-0.00636519	1.002949	0.014121	102	-0.02952588
Fe-XXIII(XXIV)	7.457	7.459 ± 0.006	-0.00617159	1.003787	0.014959	105	-0.02372392
Ni-XIX	14.060	14.109 ± 0.024	-0.00577074	1.004039	0.015210	106	-0.02117257
Fe-XXIV	10.634	10.633 ± 0.005	-0.00955665	1.004169	0.015341	106	-0.03427216
S-XV	5.055	5.050 ± 0.002	-0.01080625	1.006229	0.017400	111	-0.02956479
Fe-XXIV	7.989	7.984 ± 0.004	-0.01365020	1.006965	0.018136	113	-0.03484912
Fe-XXIV(XXIII)	11.026	11.025 ± 0.007	-0.02092979	1.010153	0.021324	119	-0.04321873
Fe-XXIV	11.432	11.465 ± 0.017	-0.01904846	1.011509	0.022681	121	-0.03693196
Mg-XII	8.421	8.425 ± 0.002	-0.01857007	1.011780	0.022952	121	-0.03560158
Fe-XXIV	11.176	11.182 ± 0.004	-0.02442425	1.012483	0.023654	122	-0.04555587
Al-XIII	7.173	7.172 ± 0.004	-0.01942630	1.013844	0.025016	124	-0.03456750
Fe-XXIV	8.316	8.309 ± 0.004	-0.02675849	1.015154	0.026325	126	-0.04579591
Mg-XII (Ni-XXVI)	7.101	7.083 ± 0.003	-0.03774527	1.022585	0.033756	133	-0.05565784

Table 1: Parameters of blue-shifted lines of the jet of SS 433 for $\beta_j \sim 0.022$. Average angle is 86° .

Identity	$\lambda_o(\text{\AA})$	$\lambda_e(\text{\AA})$	<i>hxc</i>	<i>f</i>	β	θ (deg)	a_0/w^3
FeXXV-1s ² p-1s ²	1.855	2.147 ± 0.001	0.05983618	0.823078	0.320618	245	-0.14255121
FeXXVI-Lya	1.780	2.057 ± 0.005	0.05116418	0.829972	0.313723	246	-0.12427799
NiXXVII-1s ² p-1s ²	1.592	1.836 ± 0.003	0.03968798	0.837108	0.306588	246	-0.09850676
FeXXIV	7.986	9.214 ± 0.006	0.03436392	0.841166	0.302529	247	-0.08641189
SiXIII-1s ² p-1s ²	6.675	7.747 ± 0.018	-0.02797551	0.888690	0.255005	251	0.08681686
SiXIV-Lya	6.182	7.133 ± 0.004	-0.07025553	0.917810	0.225886	255	0.27182612

Table 2: Parameters of red-shifted lines of the jet of SS433 for $\beta_j \sim 0.29$. Average angle is 248°.

Identity	$\lambda_o(\text{\AA})$	$\lambda_e(\text{\AA})$	<i>hxc</i>	<i>f</i>	β	θ (deg)	a_0/w^3
Ni-XXVIII	1.532	1.526 ± 0.005	0.08903135	0.935532	0.128936	63	-0.19850916
Ni-XXVII	1.592	1.590 ± 0.002	0.08267751	0.939096	0.125371	64	-0.19008134
Fe-XXVI	1.780	1.786 ± 0.001	0.05108051	0.960209	0.104259	70	-0.15230057
Fe-XXV	1.855	1.860 ± 0.001	0.03133152	0.975514	0.088954	77	-0.13435166
Fe-XXIII	8.815	8.851 ± 0.010	0.02612262	0.988381	0.076087	83	-0.22681902
Ni-XIX	12.435	12.426 ± 0.010	0.01795082	0.989686	0.074781	84	-0.17789672
Si-XIIIr	6.648	6.652 ± 0.002	0.00838549	0.991826	0.072642	86	-0.10972645
Ar-XVII (S-XVI)	3.962	3.970 ± 0.004	0.00938674	0.992918	0.071550	86	-0.14818177
Ar-XVIII	3.733	3.740 ± 0.003	0.00871313	0.993540	0.070928	87	-0.15634897
Ni-XXVI	9.075	9.080 ± 0.004	0.00971661	0.993659	0.070809	87	-0.17909405
Ne-X	12.134	12.146 ± 0.006	0.01102429	0.994347	0.070121	87	-0.24159577
Ca-XX	3.020	3.025 ± 0.005	0.00643031	0.994555	0.069913	88	-0.14958766
S-XVI	4.729	4.735 ± 0.001	0.00438256	0.995105	0.069363	88	-0.12195564
Ca-XIX	3.187	3.191 ± 0.004	0.00445602	0.996212	0.068256	89	-0.20838703
Fe-VIII	15.014	15.021 ± 0.029	0.00639499	0.996579	0.067889	89	-0.38865587
Si-XIV	6.182	6.186 ± 0.001	0.00296826	0.996812	0.067656	89	-0.22321473
Si-XIV	5.217	5.224 ± 0.006	0.00661529	0.997036	0.067432	89	-0.64584070
Ni-XXIII	9.529	9.538 ± 0.006	0.00431469	0.997556	0.066912	90	-1.40762246
Ni-XXVI	9.745	9.737 ± 0.007	-0.00096485	0.998554	0.065914	91	-0.08763031
Si-XIIIr	6.740	6.735 ± 0.004	-0.00369856	0.998642	0.065826	91	-0.30135897
O-VIII	16.006	16.022 ± 0.013	0.00091487	0.999368	0.065100	91	0.04008418
Fe-XXIII(XXII)	11.753	11.778 ± 0.008	0.00016857	1.000772	0.065240	93	0.00379753
Ni-XXVI(XXV)	9.372	9.371 ± 0.005	-0.00353610	1.000885	0.065353	93	-0.07661996
Ni-XXVI	9.970	9.973 ± 0.003	-0.00636519	1.002949	0.067417	94	-0.08239460
Fe-XXIII(XXIV)	7.457	7.459 ± 0.006	-0.00617159	1.003787	0.068255	95	-0.06908094
Ni-XIX	14.060	14.109 ± 0.024	-0.00577074	1.004039	0.068506	95	-0.06211102
Fe-XXIV	10.634	10.633 ± 0.005	-0.00955665	1.004169	0.068637	95	-0.10085846
S-XV	5.055	5.050 ± 0.002	-0.01080625	1.006229	0.070697	97	-0.08791105
Fe-XXIV	7.989	7.984 ± 0.004	-0.01365020	1.006965	0.071432	98	-0.10295231
Fe-XXIV(XXIII)	11.026	11.025 ± 0.007	-0.02092979	1.010153	0.074621	100	-0.12149952
Fe-XXIV	11.432	11.465 ± 0.017	-0.01904846	1.011509	0.075977	101	-0.10125270
Mg-XII	8.421	8.425 ± 0.002	-0.01857007	1.011780	0.076248	101	-0.09711047
Fe-XXIV	11.176	11.182 ± 0.004	-0.02442425	1.012483	0.076950	102	-0.12263362
Al-XIII	7.173	7.172 ± 0.004	-0.01942630	1.013844	0.078312	102	-0.09071594
Fe-XXIV	8.316	8.309 ± 0.004	-0.02675849	1.015154	0.079621	103	-0.11733112
Mg-XII (Ni-XXVI)	7.101	7.083 ± 0.003	-0.03774527	1.022585	0.087052	107	-0.12620914

Table 3: Parameters of blue-shifted lines of the jet of SS433 for $\beta_j \sim 0.076$. Average angle is 90°.

within [33°,133°] (with average angle of inclination to the line of sight being 86°) for $\beta_j \sim 0.022$, and within [63°,107°] (with average angle of inclination to the line of sight being 90°) for $\beta_j \sim 0.076$.

Evidently, the jet is narrower for higher jet velocity. Furthermore, apart from the distribution expected on the basis of Figure 2, there exist variations in line-velocities at various angular ranges. These variations get enhanced at the higher jet speed, we note.

Variations within angular ranges are also seen in the line-acceleration parameter, $\frac{a_0}{w^3}$, as shown in Figures 4 and 5. Data are fitted with cubic spline curves. (We are not using acceleration, $\frac{a_0}{w^3}$ as we have not fixed ω , the frequency of temporal variations of acceleration).

Variation of line-velocity β with parameter $\frac{a_0}{w^3}$ is then depicted in

Figure 6 for $\beta_j \sim 0.022$ and in Figure 7 for $\beta_j \sim 0.076$. Data are also fitted with cubic spline curves to indicate these variations.

Of interest to modeling of jets and considerations of their prime mover is angular distribution of elements emitting observed spectral lines. We therefore provide the angular distribution of elements in Figure 8 for $\beta_j \sim 0.022$ and in Figure 9 for $\beta_j \sim 0.076$.

Tables 2 and 4 then provide the results of analysis, following Section 2, for data on the red-shifted jet as in Marshall et al. [8].

Figure 10 then shows the angular variation of line velocities for $\beta_j \sim$

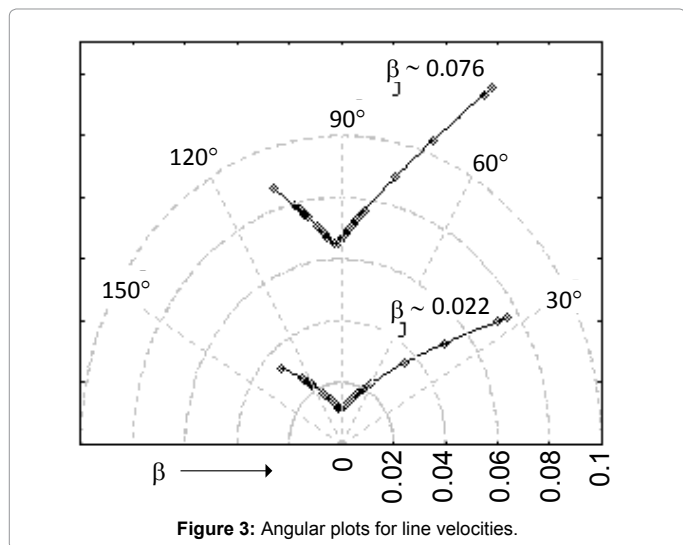


Figure 3: Angular plots for line velocities.

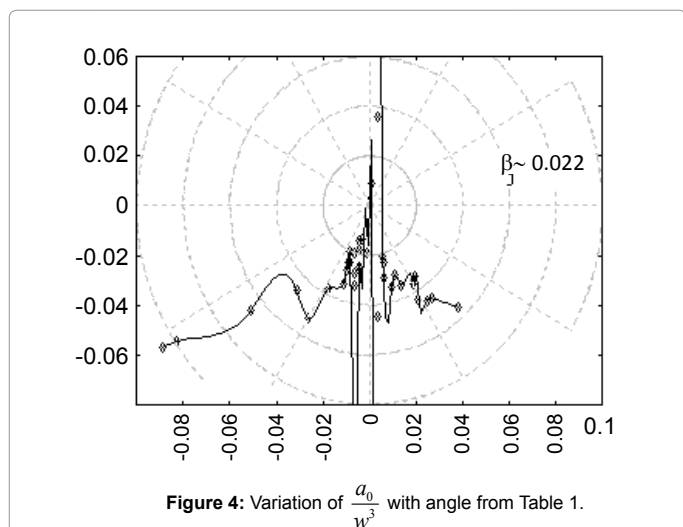


Figure 4: Variation of $\frac{a_0}{w^3}$ with angle from Table 1.

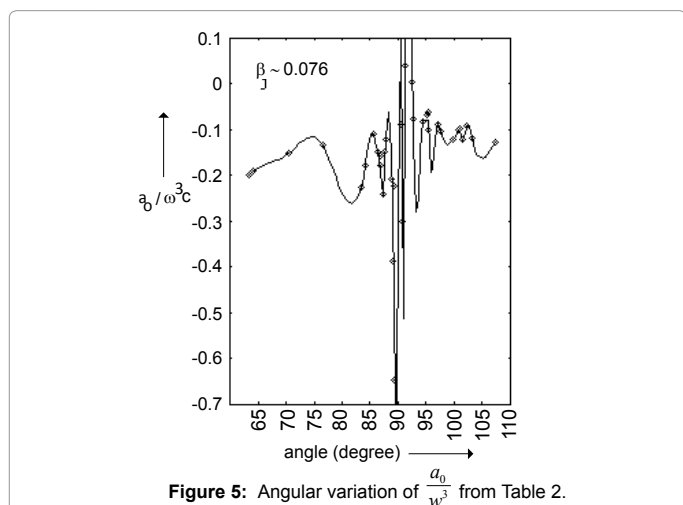


Figure 5: Angular variation of $\frac{a_0}{w^3}$ from Table 2.

0.29 (Table 2) for $\beta_j \sim 0.32$ (Table 4). Notice here that the jet velocity is substantially larger for the red-shifted jet than that for the blue-shifted jet of SS 433.

Figure 11 now shows the angular variation of the line-acceleration parameter $\frac{a_0}{w^3}$ for $\beta_j \sim 0.29$ (Table 2) and for $\beta_j \sim 0.32$ (Table 4).

Discussion

Acceleration dependence of Doppler Effect has an important consequence: the spectral shift is not dependent on only the velocity of the source. Acceleration also contributes to the spectral shift, as in eq. (4), in a significant manner.

In our analysis of the micro-quasar SS 433, we then find that acceleration plays one important role. Lines of the blue-shifted jet with

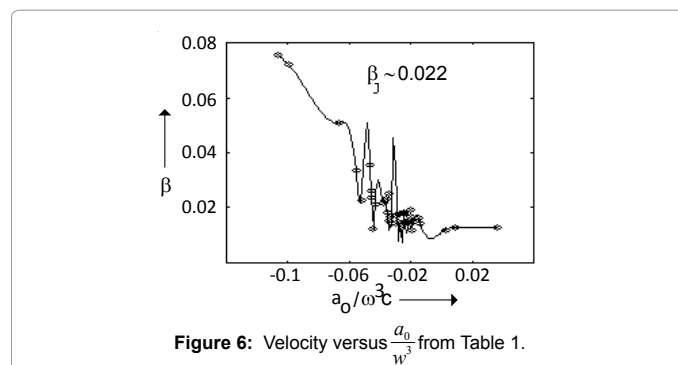


Figure 6: Velocity versus $\frac{a_0}{w^3}$ from Table 1.

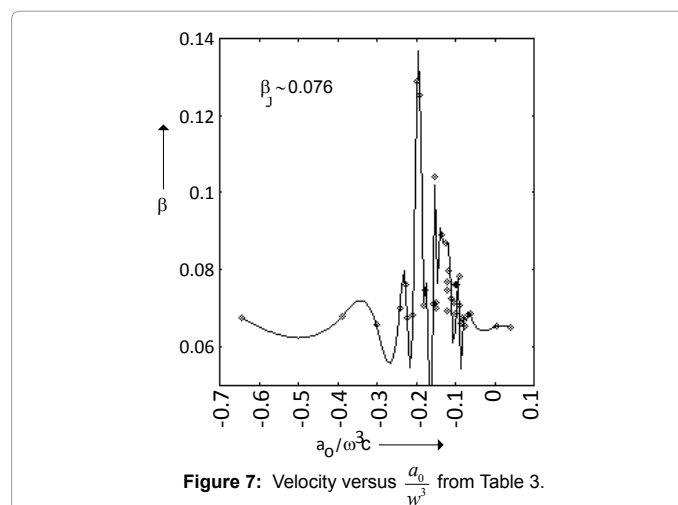


Figure 7: Velocity versus $\frac{a_0}{w^3}$ from Table 3.

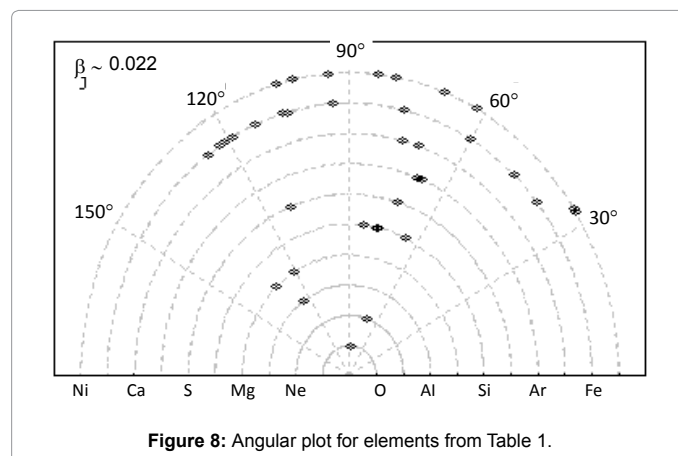


Figure 8: Angular plot for elements from Table 1.

Identity	$\lambda_o(\text{Å})$	$\lambda_r(\text{Å})$	$h\nu c$	f	β	θ (deg)	a_o/w^3
FeXXV-1s ² p-1s ²	1.855	2.147 ± 0.001	0.05983618	0.823078	0.353844	250	-0.17393410
FeXXVI-Lya	1.780	2.057 ± 0.005	0.05116418	0.829972	0.346950	250	-0.15218493
NiXXVII-1s ² p-1s ²	1.592	1.836 ± 0.003	0.03968798	0.837108	0.339814	251	-0.12111256
FeXXIV	7.986	9.214 ± 0.006	0.03436392	0.841166	0.335755	251	-0.10650083
SiXIII-1s ² p-1s ²	6.675	7.747 ± 0.018	-0.02797551	0.888690	0.288232	256	0.11138681
SiXIV-Lya	6.182	7.133 ± 0.004	-0.07025553	0.917810	0.259112	259	0.36507672

Table 4: Parameters of red-shifted lines of the jet of SS433 for $\beta_j \sim 0.32$. Average angle is 253°.

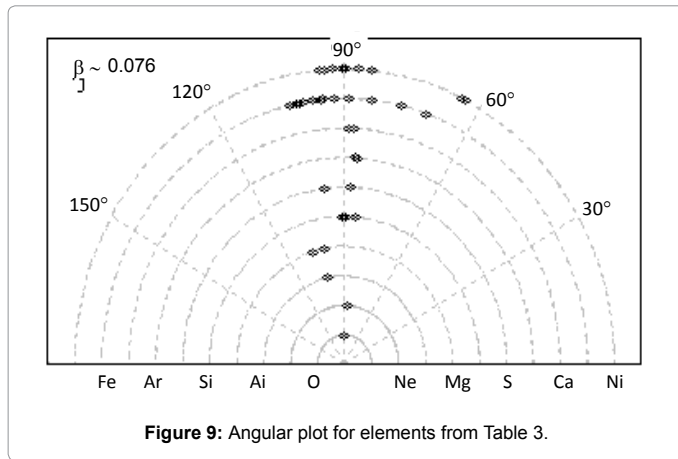


Figure 9: Angular plot for elements from Table 3.

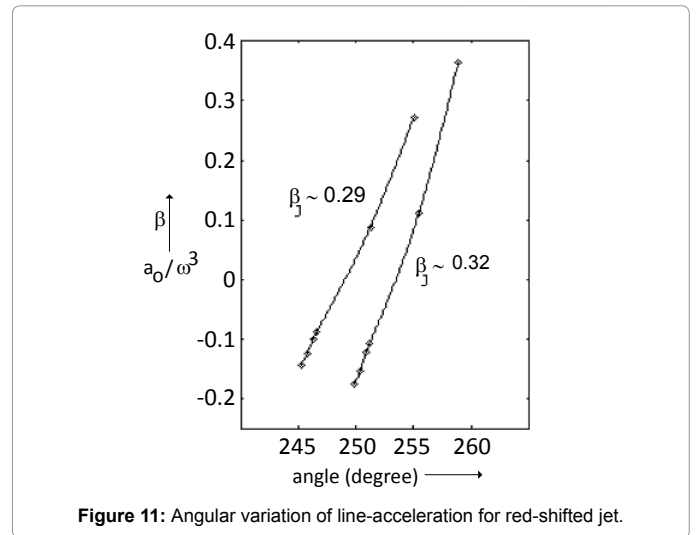


Figure 11: Angular variation of line-acceleration for red-shifted jet.

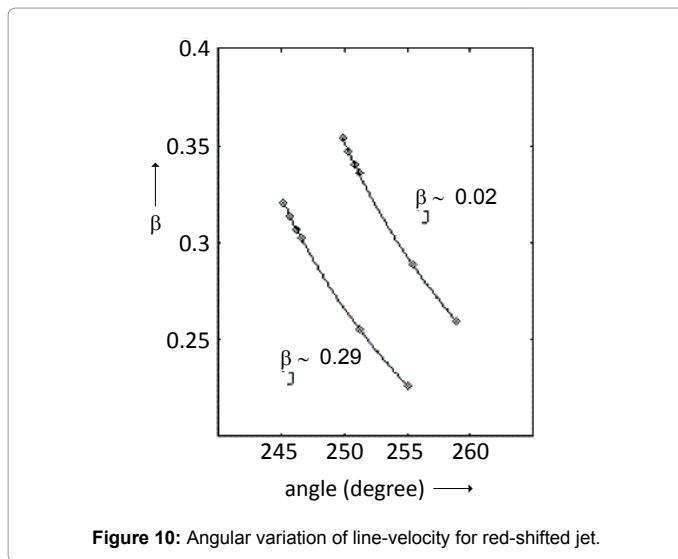


Figure 10: Angular variation of line-velocity for red-shifted jet.

$f > 1$ then correspond to angles larger than 90° to the line of sight. (For the red-shifted jet, $f > 1$ would imply angles greater than 270°, we note. However, we do not find such lines in the data on SS 433 for the red-shifted jet. However, see later, also.) This kind of identification of angle is not possible without the acceleration dependence of the Doppler shift.

From our analysis, presented in Table 1 and Table 3, we find that the speed of the blue-shifted jet is non-relativistic, that is, $\beta_j \sim 0.022$ or $\beta_j \sim 0.076$. But, the red-shifted jet is mildly relativistic $\beta_j \sim 0.29$ or $\beta_j \sim 0.32$.

As discussed in Section 2, values $\beta_j \sim 0.022$ and $\beta_j \sim 0.29$ have been obtained by adding average $\langle \beta_{min} \rangle$ of the line-values of β_{min} ; while the values of $\beta_j \sim 0.076$ and $\beta_j \sim 0.32$ have been obtained by adding maximum of the line-values of β_{min} .

We, of course, suggest the addition of the average $\langle \beta_{min} \rangle$ of the line-values of β_{min} to each of them. Maximum of β_{min} corresponds, from the analogy of a train; to maximum effect of the push material receives. We have therefore used it only to compare the jet characteristics at $\beta_j = \beta_{min}$ with those at any higher value for β_j .

We therefore measure $\beta_j \sim 0.022$ for the blue-shifted jet and $\beta_j \sim 0.029$ for the red-shifted jet as our observed values. We also find variations in line velocities in both these jets of SS 433.

We have not provided errors of various quantities here, as we find that errors do not change the main conclusions of our analysis in any significant manner. That the speed of the blue-shifted jet is substantially non-relativistic, that the speed of the blue-shifted jet is different than that of the red-shifted jet, that there are interesting variations of line-velocity, etc. hold.

The bulk flow speed of the material 0.26c of the blue-shifted jet is, in particular, substantially smaller than obtained [7] from the standard analysis with no acceleration dependence of the Doppler shift. Nevertheless, the bulk flow speed, $\beta_j \sim 0.029$, of the red-shifted jet is close to this value, we then note.

We therefore find blue-shifted and red-shifted jets to be possessing different speeds in the system of SS 433. Then, any model assuming the same speed for the two oppositely directed jets appears to be in difficulty here.

But, we could be viewing an early (meaning “closer” to the prime mover) part of the receding jet (for which the speed is higher) and the later (meaning “away from” the prime mover) part of the approaching jet (for which the speed is lower as a result of its passage through matter), perhaps. This could then be a possible reason for difference in speeds of the (blue-shifted) approaching and (red-shifted) receding jets.

Angular dependence of the line-acceleration parameter $\frac{a_0}{w^3}$ of Figure 4 and the dependence of line-velocity β_L on the line-acceleration parameter of Figure 6 are of definite significance, now.

In this context, we note that variations of $\frac{a_0}{w^3}$ correspond directly with those of $\frac{a_0}{w^3}$, the line-acceleration. We can, consequently, interpret these variations as providing us the angular distribution of the clouds causing deceleration of the jet material.

We emphasize then that the multi-epoch monitoring of these variations will provide us valuable information on the jet advance and the parameters of these jet-obstructing clouds. Furthermore, such monitoring will also provide us information about temporal character of the activity of the prime mover of these jets, we emphasize.

Now, just the line Doppler shifts do not provide us any information on the radial distance of the jet material from its prime mover. Nevertheless, the angular distribution of elements in Figure 8 is of definite significance for it shows us the shell encountered by the jet.

Lastly, Marshall et al. [7] have also observed aperiodic variability of Doppler shifts (of blue-shifted jet) over timescale much shorter than any of the known periodicities in the system, like that of precession, orbit, and nutation. We then only note here that aperiodic variability could come from the material of jet experiencing aperiodic changes of deceleration. Any aperiodic variability of acceleration could then be related to the mechanisms of the jet acceleration and deceleration, both.

In summary, we find that analysis of data on Doppler-shifted lines of SS 433, specifically X-ray emission lines seen using *Chandra* HETGS, implies non-relativistic speed of the material of the jet causing their

emission. Our results have consequences for the energetics of the prime mover as well as for the model of the jets in SS 433.

Detailed model of the jets in SS 433 consistent with the aforementioned results of observational nature is a subject of our separate considerations.

References

1. Margon B (1984) Observations of SS 433. ARA&A 22: 507-536.
2. Mirabel IF (1999) Sources of relativistic Jets in the Galaxy. ARA&A 37: 409-443.
3. Fabrika S (2004) Properties of SS 433 and ultraluminous X-ray sources in external galaxies. Astrophysics and Space Physics Reviews 12, 1.
4. Margon, B, Anderson SF (1989) Ap J, 347, 448.
5. Blundell KM, Bowler MG (2005) Jet Velocity in SS 433: Its Anticorrelation with Precession-Cone Angle and Dependence on Orbital Phase. Ap J 622: L129-L132.
6. Stirling AM, Jowett FH, Spencer RE, Paragi Z, Ogle RN, et al. (2002) Radio-emitting component kinematics in SS433. MNRAS 337: 657-665.
7. Marshall HL, Canizares CR, Hillwig T, Mioduszewski A, Rupen M, et al. (2013) Multi-wavelength Observations of the SS433 Jets (To be published Ap J) (arxiv.org: astro-ph.HE/1307.8427).
8. Marshall HL, Canizares CR, Schulz NS (2002) The High-Resolution X-Ray Spectrum of SS 433 Using the Chandra HETGS. A J 564: 941-952.
9. Wagh SM (2013a) Pramana 81(3): 439-448. (doi:10.1007/s12043-013-0584-6).
10. Wagh SM (2013b) J Modern Physics 4(8A): 102-104. (doi:10.4236/jmp.2013.48A008).
11. Wagh SM (2013c) "Subtlety in relativity", Proceedings of SPIE Conference on The Nature of Light: What are photons? Paper no. 8832-25, San Diego, California, 25-29 August 2013.
12. Wagh SM (2013d) "Measuring velocity and acceleration using Doppler shift of a source with an example of Jet in SS433", submitted for publication.